Mech. Engg. Res. Bull
Vol. 12, (1989), pp. 55-69

Application of Cascade Theory for the Performance Prediction of Darrieus Turbines with Blades of Cambered Cross-Section

N. R. Dhar *
A. C. Mandal **

ABSTRACT

The performance prediction of vertical-axis straight-bladed Darrieus wind turbines with blades of cambered cross-section is performed based on cascade principle similar to that used in turbomachines. The correlation of the calculated results including blades of cambered cross-section with those including blades of symmetric cross-section show that there occur improvement in power characteristics if blades of cambered cross-section are applied.

NOMENCLATURE

A	projected frontal area of turbine
AR	aspect ratio = H/C
C	blade chord
C_d	blade drag coefficient
C_D	overall drag coefficient
C_l	blade lift coefficient
C_n	normal force coefficient
C_P	overall power coefficient = $P_o/(1/2\,\rho\, AV_\infty^3)$
C_Q	overall torque coefficient
C_t	tangential force coefficient
D	Blade drag force
f	maximum camber
F_n	normal force (in radial direction)
F_n^+	local non-dimensional normal force $= C_n\,(W/V_\infty)^2$
F_{nid}	force appearing in frictionless flow
F_{nv}	force due to pressure loss
F_t	tangential force
F_t^+	local non-dimensional tangential force $= C_t\,(W/V_\infty)^2$
H	height of turbine
K_i	exponent in the induced velocity relation
L	blade lift force
L_{id}	lift force appearing in frictionless flow
L_v	lift force contributed by pressure loss
$\dot{m}$	mass flow rate
N	number of blades

*Department of Mechanical Engineering, Bangladesh Institute of Technology, Khulna
** Department of Mechanical Engineering, Bangladesh University of Engineering and Technology, Dhaka-1000.

P	static pressure	
P_o	overall power	
P_∞	atmospheric pressure	
Q	overall torque	
R	turbine radius at equator	
R_{et}	turbine speed Reynolds Number = $R\omega C/\upsilon$	
R_{ew}	wind speed Renolds Number = $V_\infty C/\upsilon$	
t	blade spacing = $(2\pi R/N)$	
V_a	induced velocity	
V_e	wake velocity in upstream side	
V_w	wake velocity in downstream side	
V_Γ	velocity contributed by circulation	
V_∞	wind velocity	
W	relative flow velocity	
W_o	relative flow velocity appearing in rectilinear flow	
α	angle of attack	
α_o	angle of attack in rectilinear flow	
γ_p	blade pitch angle	
Γ	circulation per unit length	
ΔP_{ov}	total pressure loss term (total cascade loss)	
ε	D/L	
θ	azimuth angle	
λ	tip speed ratio = $R\omega/V_\infty$	
υ	kinematic viscosity	
ρ	fluid density	
σ	solidity = NC/R	
ω	angular velocity of turbine in rad/sec.	

Subscript

d	downstream side
u	upstream side
x,y	x-axis, y-axis
1,2	cascade inlet, cascade outlet

1. INTRODUCTION

The cascade theory presented by Hirsch and Mandal [1] is applied for the performance prediction of vertical-axis straight bladed Darrieus wind turbines. In order to eliminate the convergence problem associated with the momentum theory especially for a turbine with high solidity, higher blade pitching and at higher tip speed ratio and to avoid vortex model which cannot always predict performance reasonably, rather it often creates convergence problem and consumes very high computation time, the cascade theory is used in this analysis.

The analysis incorporates the turbine blades of cambered cross-section in place of conventional symmetric one. Using blades of cambered cross-section, the lift forces increase in the upstream side and decrease in the downstream side in general if compared to those for a turbine with blades of symmetric cross-section. As a result higher power is produced in the upstream side and lower power is produced in the downstream side if compared to those produced by the turbine with blades of symmetric cross section. However, the net power production of the turbine with blades of cambered cross-section is always higher than that with blades of symmetric cross-section.

Aspect ratio effect is encountered in the analysis in accordance with the reference [2]. The effect of zero-lift drag coefficient is taken into account in the calculation referring to the model presented by Hirsch and Mandal [3]. References [4], [5], [6] and [7] are consulted in order to consider the lift-drag characteristics in the calculation.

2. AERODYNAMIC THEORY

2.1 Blade Angles and Velocities

The expressions of angle of attack and relative flow velocity for upstream side may be written as, referring to the figures 1 and 2,

$$\alpha_{au} = \tan^{-1}\left[\frac{\sin\theta}{\frac{R\omega}{V_\infty} / \frac{V_{au}}{V_\infty} + \cos\theta}\right] \tag{1}$$

$$\frac{W_{ou}}{V_\infty} = \frac{V_{au}}{V_\infty}\sqrt{\left[\left(\frac{R\omega}{V_\infty} / \frac{V_{au}}{V_\infty}\right) + \cos\theta\right]^2 + \sin^2\theta} \tag{2}$$

For downstream side similar expressions of angle of attack and relative flow velocity are obtained.

The Darrieus turbine is assumed in the form of cascade after finding the angle of attack and relative flow velocity as shown in the figure 3. The cascade is considered in a plane normal to the turbine axis. If the blade represented by (1) at an azimuthal angle θ is considered as the reference blade, the flow conditions on the other two blades represented by (2) and (3) are assumed to be equal to those of the reference blade. This process is continued for one complete revolution of the reference blade with a step of $\delta\theta$.

In the following analysis, the general mathematical expressions are obtained, for upstream and downstream sides by omitting the subscripts u and d. However, these expressions may be applied for upstream and downstream sides by subscripting the variable parameters (dependent on sides of turbines) with u for upstream and d for downstream.

The velocity diagram on the reference blade element of the cascade configuration is shown in the figure 4. A control surface is considered in this figure consisting of two lines parallel to the cascade front and two identical streamlines having interspace t.

The relative flow velocities (W_1, W_2) and the angles of attack (α_1, α_2) at the cascade inlet and outlet may be determined from the figure 4. Blade element upstream and downstream sides are respectively termed as cascade inlet and outlet. W_1, W_2 , α_1 and α_2 are expressed as,

$$\frac{W_1^2}{V_\infty^2} = \frac{W_x^2}{V_\infty^2} + \frac{(W_y - V_\Gamma)^2}{V_\infty^2} \qquad (3)$$

$$\frac{W_2^2}{V_\infty^2} = \frac{W_x^2}{V_\infty^2} + \frac{(W_y + V_\Gamma)^2}{V_\infty^2} \qquad (4)$$

$$\alpha_1 = \tan^{-1}\left[\frac{W_x / V_\infty}{(W_y - V_\Gamma) / V_\infty}\right] \qquad (5)$$

$$\alpha_2 = \tan^{-1}\left[\frac{W_x / V_\infty}{(W_y + V_\Gamma) / V_\infty}\right] \qquad (6)$$

where V_Γ is the velocity contributed by circulation ΓH. V_Γ is written as,

$$V_\Gamma = \frac{\Gamma H}{2t} = \frac{N\Gamma H}{4\pi R} \qquad (7)$$

2.2 Aerodynamic Force:

Along the bounding streamlines the pressure forces are cancelled (figure 4), viscous forces can be neglected outside the boundary layers. Only there remains the momentum flux through the straight lines parallel to the cascade front. So the force in the tangential direction due to the rate of change of momentum is obtained as,

$$F_t = \mathring{m}\,(W_2 \cos\alpha_2 - W_1 \cos\alpha_1) \qquad (8)$$

Applying the continuity equation, the mass flow rate $\mathring{m}$ can be determined as,

$$\mathring{m} = \rho Ht\, W_1 \sin\alpha_1 = \rho Ht\, W_2 \sin\alpha_2 = \rho Ht\, W_x \qquad (9)$$

The force in the normal direction to the cascade may be found as,

$$F_n = \mathring{m}(W_1 \sin\alpha_1 - W_2 \sin\alpha_2) + Ht\,(P_1 - P_2) \qquad (10)$$

Considering the total cascade loss by a total pressure loss term ΔP_{ov} and using Bernoulli's equation between the cascade inlet and outlet, one obtains,

$$P_1 - P_2 = \frac{\rho}{2}(W_2^2 - W_1^2) + \Delta P_{ov} \qquad (11)$$

2.3 Velocity Contributed by Circulation:

The circulation about the blade profile is defined as,

$$\Gamma = \oint \overline{W}\, \overline{ds} \qquad (12)$$

Its contribution along the streamlines is cancelled by virtue of the opposing directions of S, while the contribution along the parallel direction of the cascade front is retained. As a result the circulation becomes,

$$\Gamma = t\,(W_2 \cos\alpha_2 - W_1 \cos\alpha_1) \qquad (13)$$

From the equations (8), (9) and (13), one may obtain,

$$F_t = \rho W_x \Gamma H \qquad (14)$$

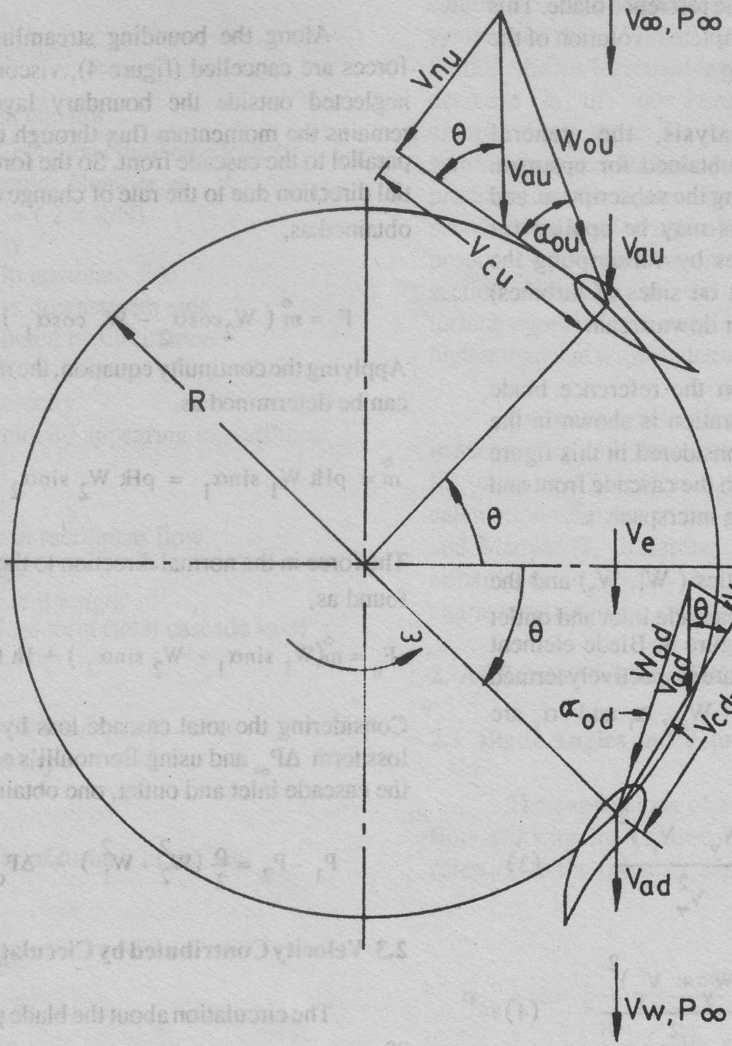

Figure 1 : Horizontal section of a straight-bladed Darrieus Turbine showing flow velocity

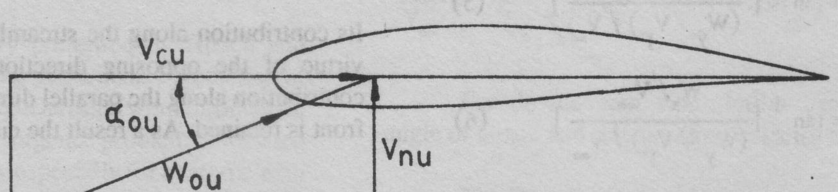

Figure 2: Relative flow velocity on a Cambered blade airfoil

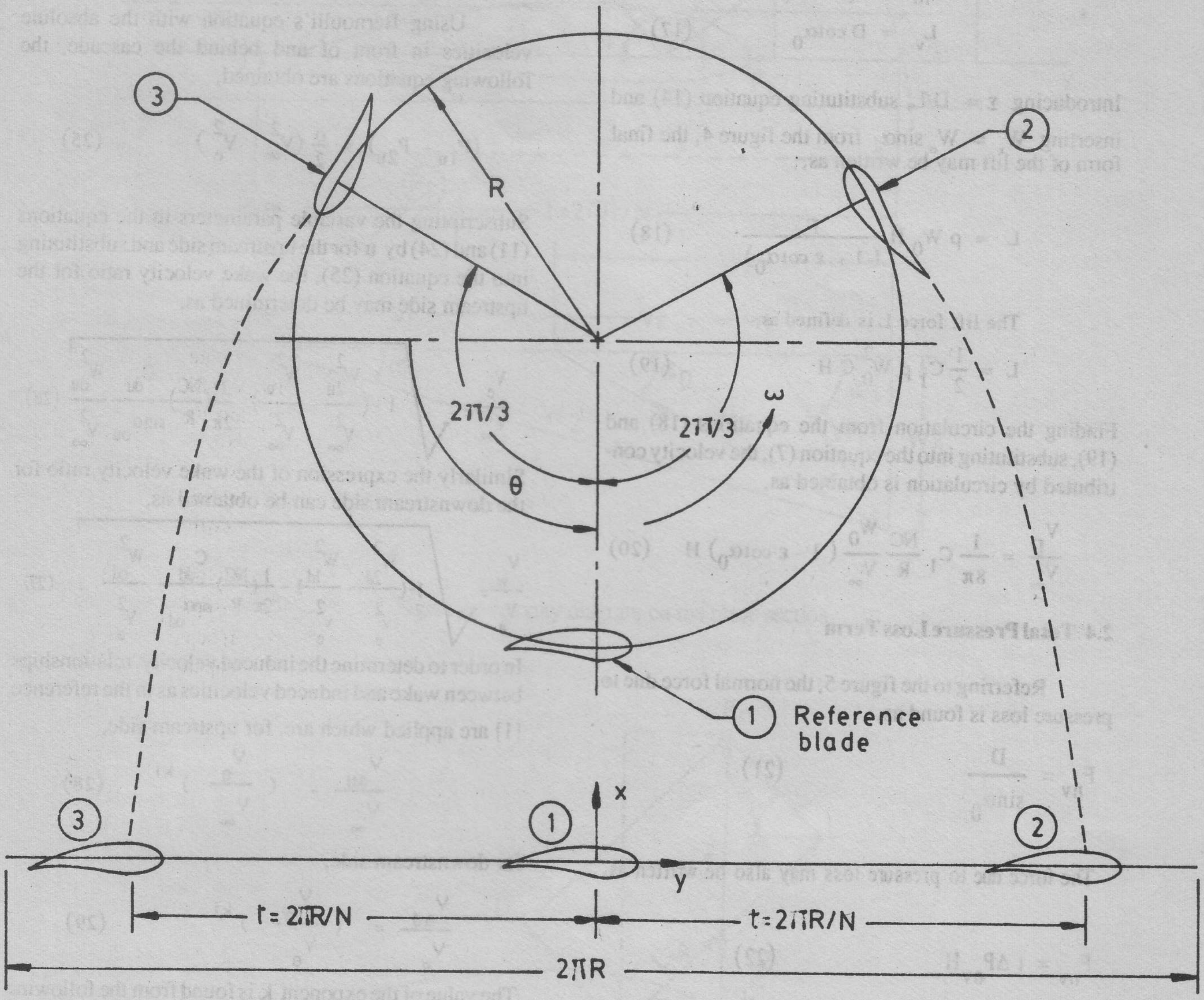

Figure 3: Development of blades into cascade configuration.

Referring to the figure 5, the lift force can be found as,

$$L = L_{id} + L_v \tag{15}$$

where, $L_{id} = F_t / \sin\alpha_0$ (16)

$L_v = D \cot\alpha_0$ (17)

Introducing $\varepsilon = D/L$, substituting equation (14) and inserting $W_x = W_o \sin\alpha_o$ from the figure 4, the final form of the lift may be written as,

$$L = \rho W_0 H \frac{\Gamma}{(1 - \varepsilon \cot\alpha_0)} \tag{18}$$

The lift force L is defined as,

$$L = \frac{1}{2} C_1 \rho W_0^2 C H \tag{19}$$

Finding the circulation from the equations (18) and (19), substituting into the equation (7), the velocity contributed by circulation is obtained as,

$$\frac{V_\Gamma}{V_\infty} = \frac{1}{8\pi} C_1 \frac{NC}{R} \frac{W_0}{V_\infty} (1 - \varepsilon \cot\alpha_0) H \tag{20}$$

2.4 Total Pressure Loss Term

Referring to the figure 5, the normal force due to pressure loss is found as,

$$F_{nv} = \frac{D}{\sin\alpha_0} \tag{21}$$

The force due to pressure loss may also be written as,

$$F_{nv} = t \Delta P_{ov} H \tag{22}$$

The drag force D is defined as,

$$D = \frac{1}{2} C_d \rho W_0^2 C H \tag{23}$$

From the equations (21), (22) and (23), the pressure loss term may be expressed, introducing $t = 2\pi R/N$, as,

$$\frac{\Delta P_{ov}}{\rho V_\infty^2} = \frac{1}{4\pi} \frac{C_d}{\sin\alpha_0} \frac{NC}{R} \frac{W_0^2}{V_\infty^2} \tag{24}$$

2.5 Velocity Ratios

Using Bernoulli's equation with the absolute velocities in front of and behind the cascade, the following equations are obtained,

$$(P_{1u} - P_{2u}) = \frac{\rho}{2} (V_\infty^2 - V_e^2) \tag{25}$$

Subscripting the variable parameters in the equations (11) and (24) by u for the upstream side and substituting into the equation (25), the wake velocity ratio for the upstream side may be determined as,

$$\frac{V_e}{V_\infty} = \sqrt{1 - \left(\frac{W_{2u}^2}{V_\infty^2} - \frac{W_{1u}^2}{V_\infty^2}\right) - \frac{1}{2\pi}\left(\frac{NC}{R}\right)\frac{C_{du}}{\sin\alpha_{ou}} \frac{W_{ou}^2}{V_\infty^2}} \tag{26}$$

Similarly the expression of the wake velocity ratio for the downstream side can be obtained as,

$$\frac{V_w}{V_e} = \sqrt{1 - \left(\frac{W_{2d}^2}{V_e^2} - \frac{W_{1d}^2}{V_e^2}\right) - \frac{1}{2\pi}\left(\frac{NC}{R}\right)\frac{C_{dd}}{\sin\alpha_{od}} \frac{W_{od}^2}{V_e^2}} \quad \ldots \tag{27}$$

In order to determine the induced velocity, relationships between wake and induced velocities as in the reference [1] are applied which are, for upstream side,

$$\frac{V_{au}}{V_\infty} = \left(\frac{V_e}{V_\infty}\right)^{ki} \tag{28}$$

for downstream side,

$$\frac{V_{ad}}{V_e} = \left(\frac{V_w}{V_e}\right)^{ki} \tag{29}$$

The value of the exponent k_i is found from the following relation in accordance with the reference [1].

$$k_i = (.425 + .332\,\sigma) \tag{30}$$

where $\sigma = NC/R$ is the solidity of Darrieus turbine.

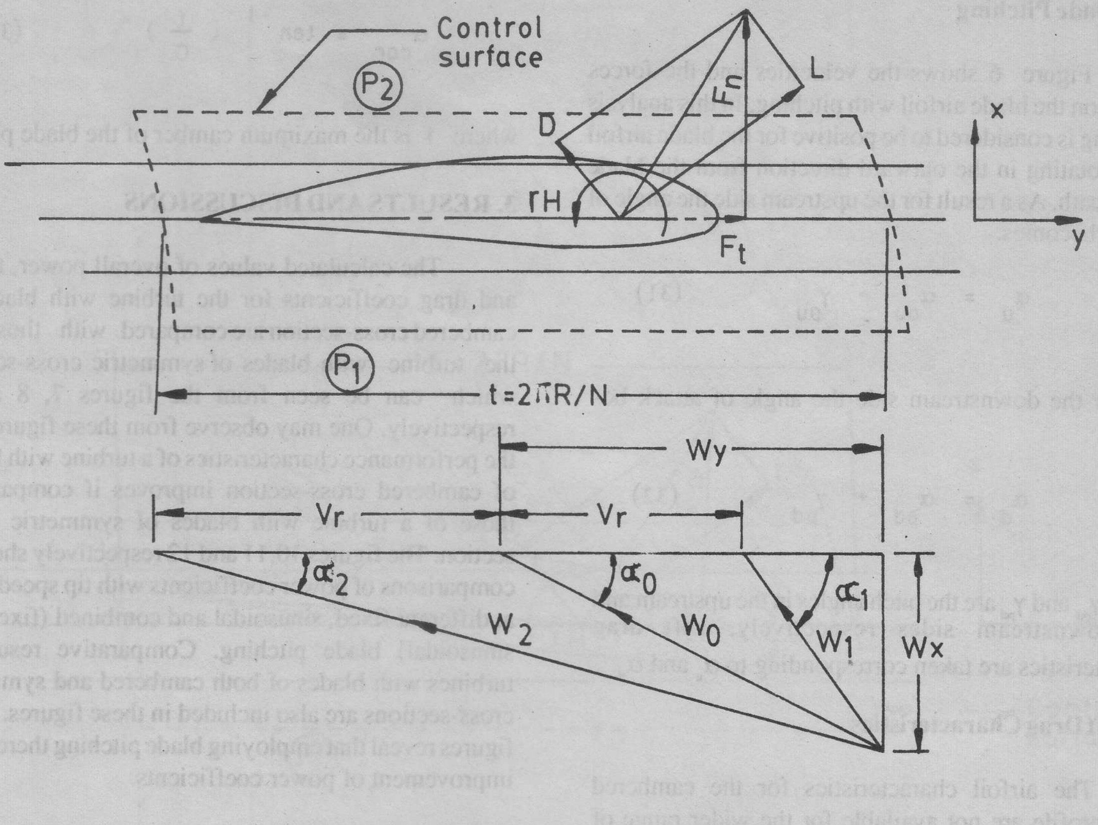

Figure 4: velocity diagram on the blade section.

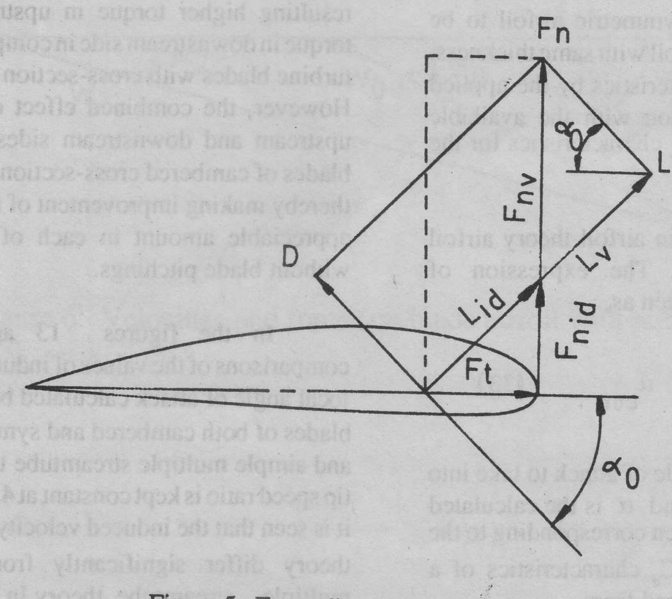

Figure 5: Force diagram on the blade section.

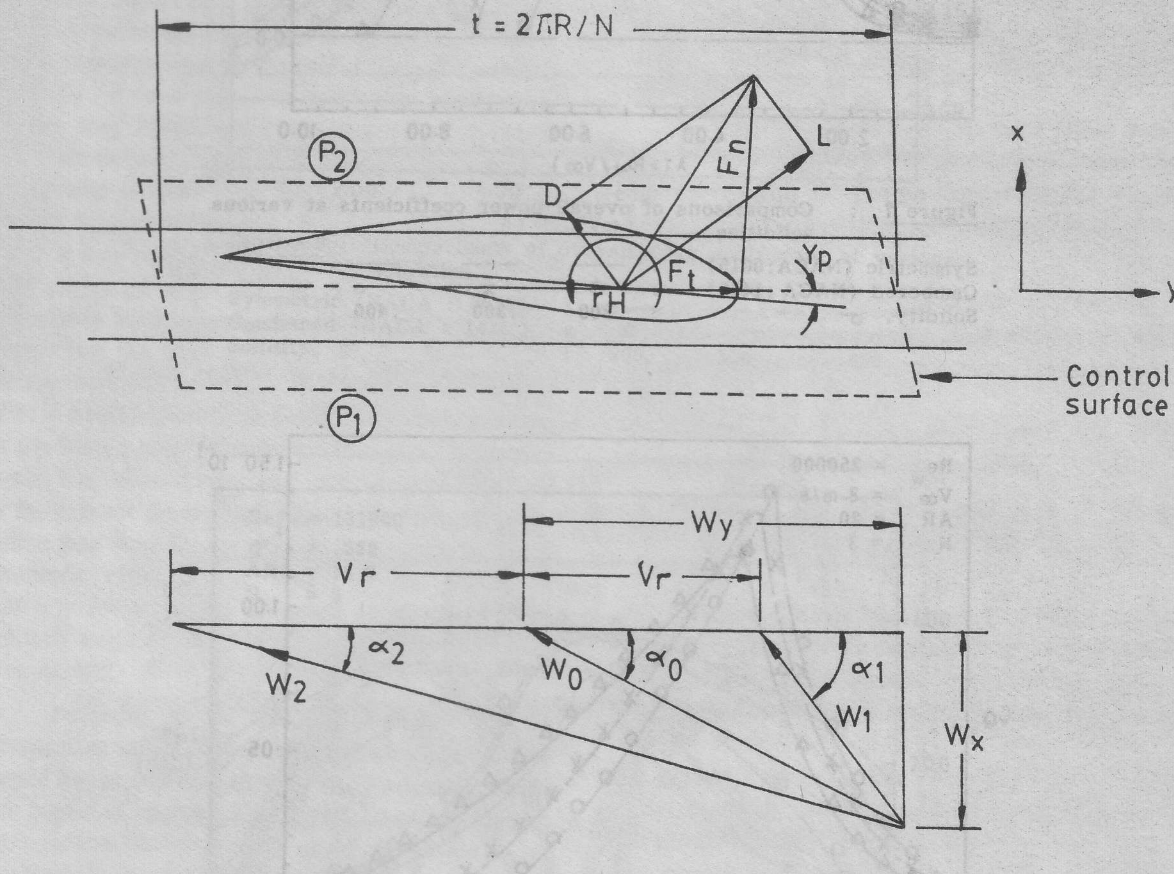

Figure 6: Velocities and forces on blade airfoil with pitching.

2.6 Blade Pitching

Figure 6 shows the velocities and the forces acting on the blade airfoil with pitching. In this analysis pitching is considered to be positive for the blade airfoil nose rotating in the outward direction from the blade flight path. As a result for the upstream side the angle of attack becomes.

$$\alpha_u = \alpha_{ou} - \gamma_{pu} \tag{31}$$

and for the downstream side the angle of attack becomes,

$$\alpha_d = \alpha_{od} + \gamma_{pd} \tag{32}$$

where γ_{pu} and γ_{pd} are the pitch angles in the upstream and the downstream sides respectively. Lift drag characteristics are taken corresponding to α_u and α_d.

2.7 Lift Drag Characteristics

The airfoil characteristics for the cambered blade profile are not available for the wider range of Reynolds number and the angles of attack. But these are necessary in the calculation of performance prediction. As a result a method is developed in order to modify the lift drag characteristics of a symmetric airfoil to be applicable for the cambered airfoil with same thickness. The calculated lift drag characteristics by the applied method give excellent correlation with the available experimental values of C_L - C_d characteristics for the cambered airfoil.

Using the concept of thin airfoil theory airfoil characteristics are modified. The expression of modified angle of attack is written as,

$$\alpha_{mod} = \alpha + \alpha_{cor} \tag{33}$$

where α_{cor} is the corrected angle of attack to take into account of camberness effect and α is the calculated angle of attack. C_L - C_d are chosen corresponding to the value of α_{mod} from the C_L - C_d characteristics of a symmetric airfoil. α_{cor} is obtained from,

$$\alpha_{cor} = \tan^{-1}\left(\frac{f}{C}\right) \tag{34}$$

where f is the maximum camber of the blade profile.

3. RESULTS AND DISCUSSIONS

The calculated values of overall power, torque and drag coefficients for the turbine with blades of cambered cross-section are compared with those for the turbine with blades of symmetric cross-section, which can be seen from the figures 7, 8 and 9 respectively. One may observe from these figures that the performance characteristics of a turbine with blades of cambered cross-section improves if compared to those of a turbine with blades of symmetric cross-section. The figures 10,11 and 12 respectively show the comparisons of power coefficients with tip speed ratios at different fixed, sinusoidal and combined (fixed plus sinusoidal) blade pitching. Comparative results of turbines with blades of both cambered and symmetric cross-sections are also included in these figures. These figures reveal that employing blade pitching there occur improvement of power coefficients.

In general for the turbine blades with cross-section of cambered profile, lift values increase in the upstream side and decrease in the downstream side resulting higher torque in upstream side and lower torque in downstream side in comparison to those for the turbine blades with cross-section of symmetric profile. However, the combined effect on torque due to the upstream and downstream sides of the turbine with blades of cambered cross-section creates higher torque thereby making improvement of rotor power but not in appreciable amount in each of the cases with and without blade pitchings.

In the figures 13 and 14 respectively, comparisons of the values of induced velocity ratios and local angle of attack calculated by cascade theory with blades of both cambered and symmetric cross-sections and simple multiple streamtube theory are made. The tip speed ratio is kept constant at 4.5. From the figure 13, it is seen that the induced velocity ratios by the cascade theory differ significantly from those by simple multiple streamtube theory.In the simple multiple

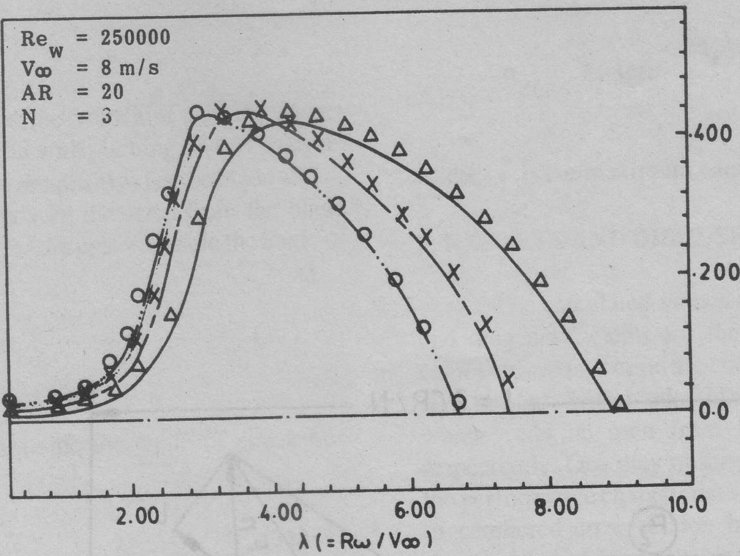

Figure 7 : Comparisons of overall power coefficients at various solidities.

Symmetric (NACA:0015)	:	———	— — —	—.·.—
Cambered (NACA:1415)	:	Δ	x	o
Solidity, σ	:	.200	.300	.400

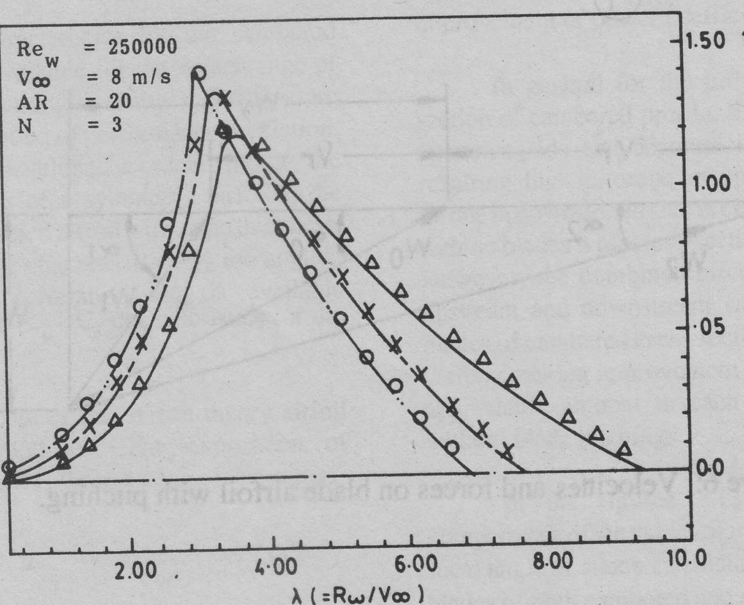

Figure 8 : Comparisons of overall torque coefficients at various solidities.

Symmetric (NACA : 0015)	:	———	— - —	—.·.—
Cambered (NACA : 1415)	:	Δ	x	o
Solidity, σ	:	.200	.300	.400

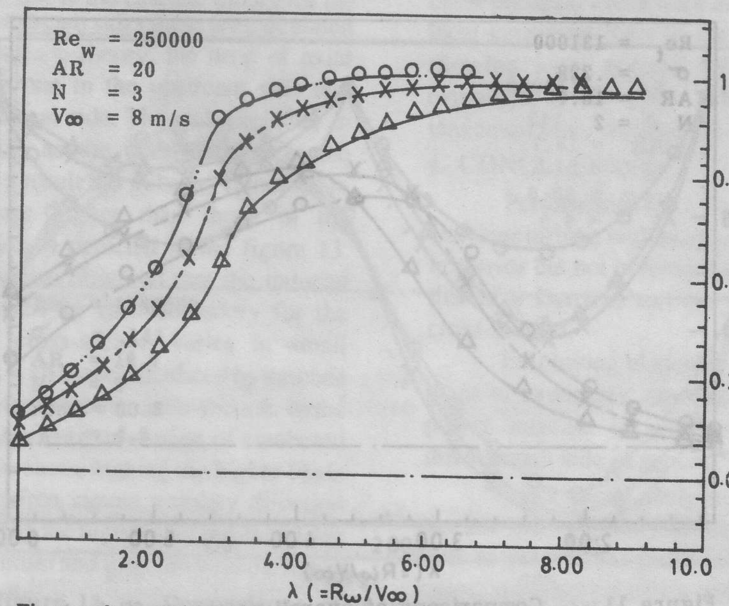

Figure 9 : Comparisons of overall drag coefficient at various solidities.

Symmetric (NACA : 0015) : ——
Cambered (NACA : 1415) : –·–
Solidity, σ : Δ .200, x .300, o .400

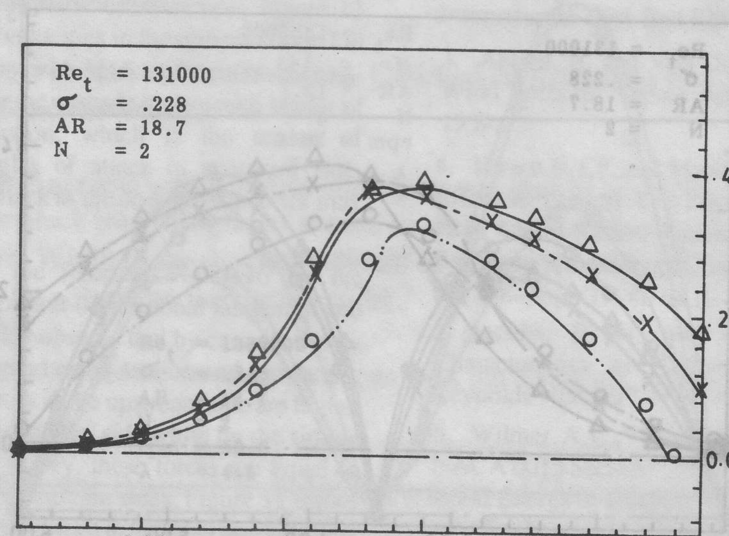

Figure 10 : Comparisons of overall power coefficients with tip speed ratios at different fixed blade pitchings.

Symmetric (NACA : 0015) : ——
Cambered (NACA : 1415) : – – –
γ_p, fixed (in deg.) : Δ o, x 3, o 6

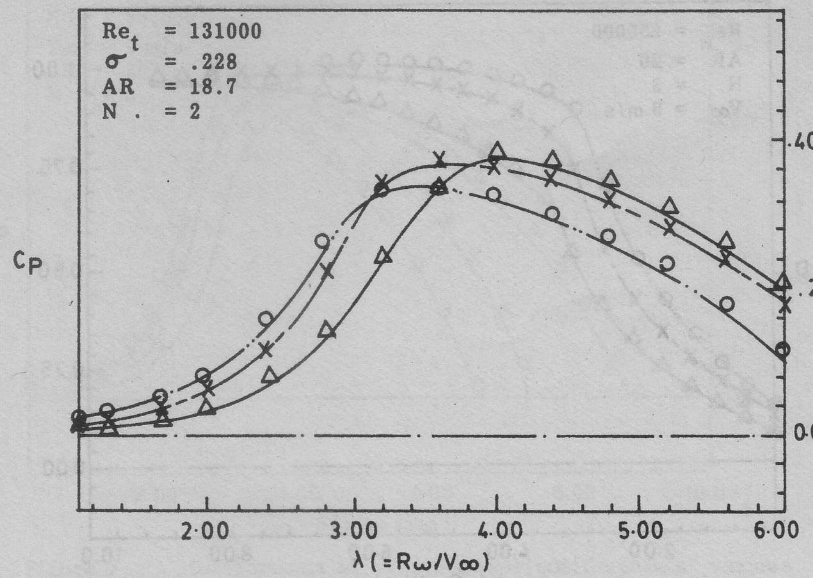

Figure 11 : Comparisons of overall power coefficients with tip speed ratios at different amplitudes of sinusoidal pitch variation.

Symmetric (NACA ; 0015)	:	———	— — —	—··—
Cambered (NACA : 1415)	:	Δ	x	o
γ_p, sinusoidal(in deg.)	:	o	3 sinθ	6 sinθ

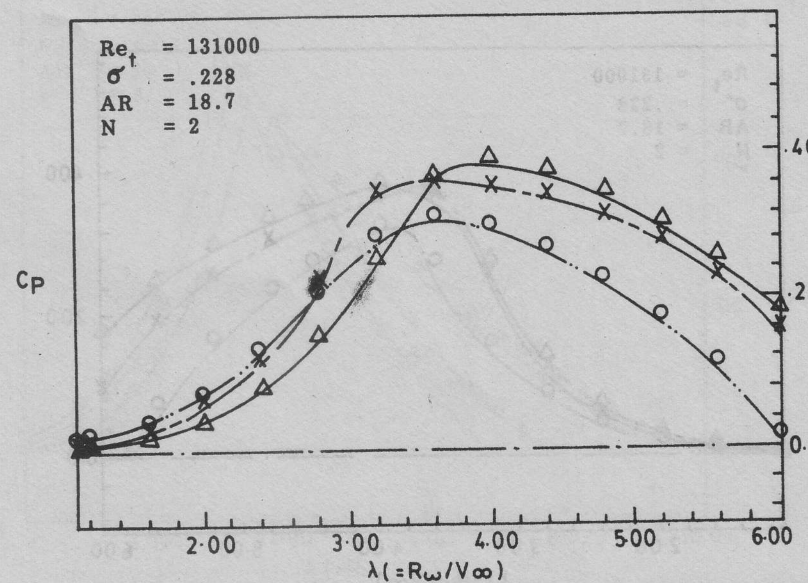

Figure 12 : Comparisons of overall power coefficients with tip speed ratios at different combined (fixed plus sinusoidal) pitch variation.

Symmetric (NACA : 0015)	:	———	— — —	—··—
Cambered (NACA : 1415)	:	Δ	x	o
γ_p, combined (in deg.)	:	o	(3+3 sinθ)	(6+6 sinθ)

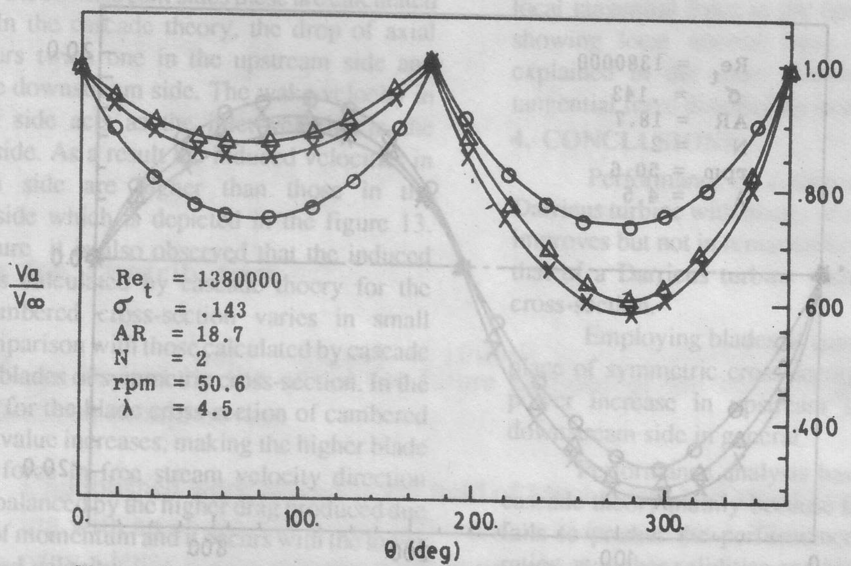

Figure 13 : Comparisons of induced velocity ratios.

Δ calc. (cascade theory ; NACA : 0015)
x calc. (cascade theory ; NACA : 1415)
o calc. (simple multiple streamtube theory; NACA:0015)

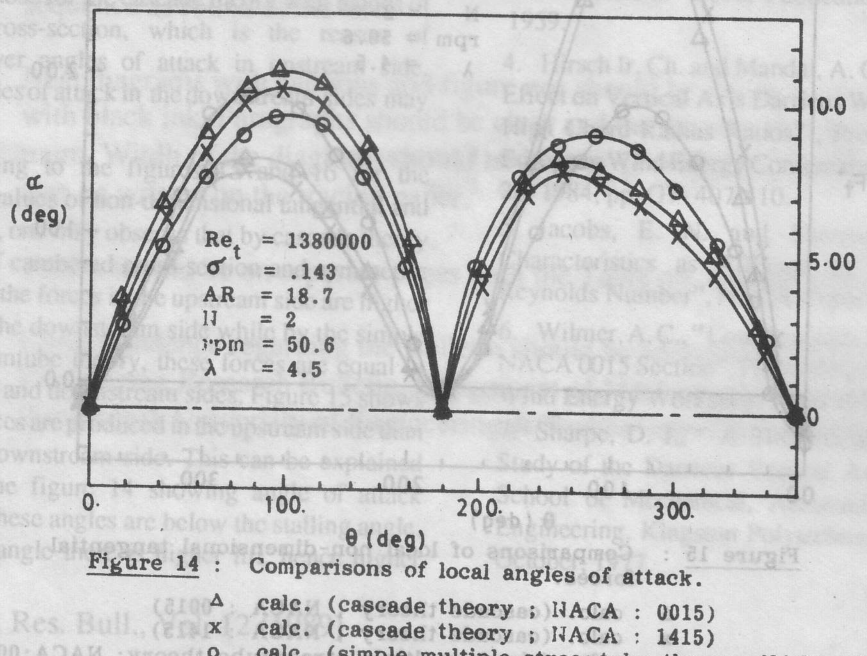

Figure 14 : Comparisons of local angles of attack.

Δ calc. (cascade theory ; NACA : 0015)
x calc. (cascade theory ; NACA : 1415)
o calc. (simple multiple streamtube theory; NACA:0015)

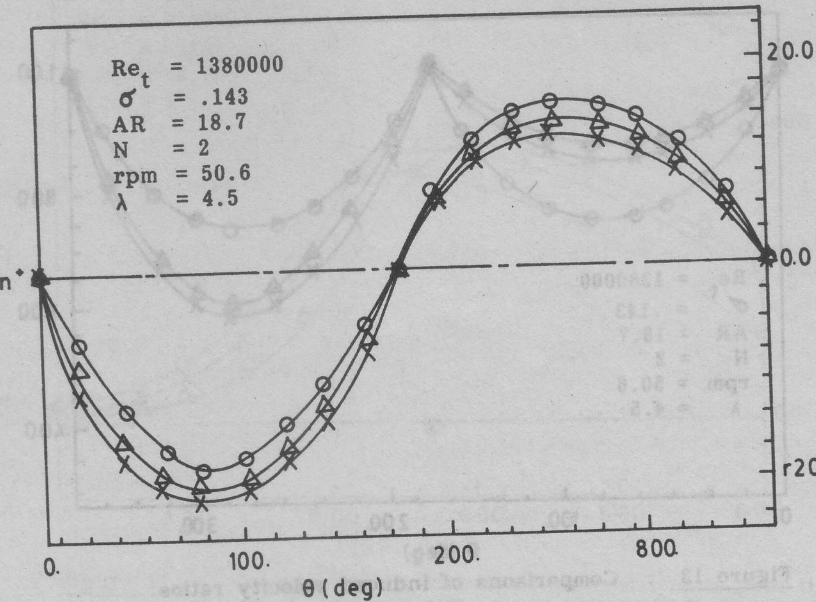

Figure 16 : Comparisons of local non-dimensional normal forces.
Δ calc. (cascade theory ; NACA : 0015)
x calc. (cascade theory ; NACA : 1415)
o calc. (simple multiple streamtube theory; NACA:0015)

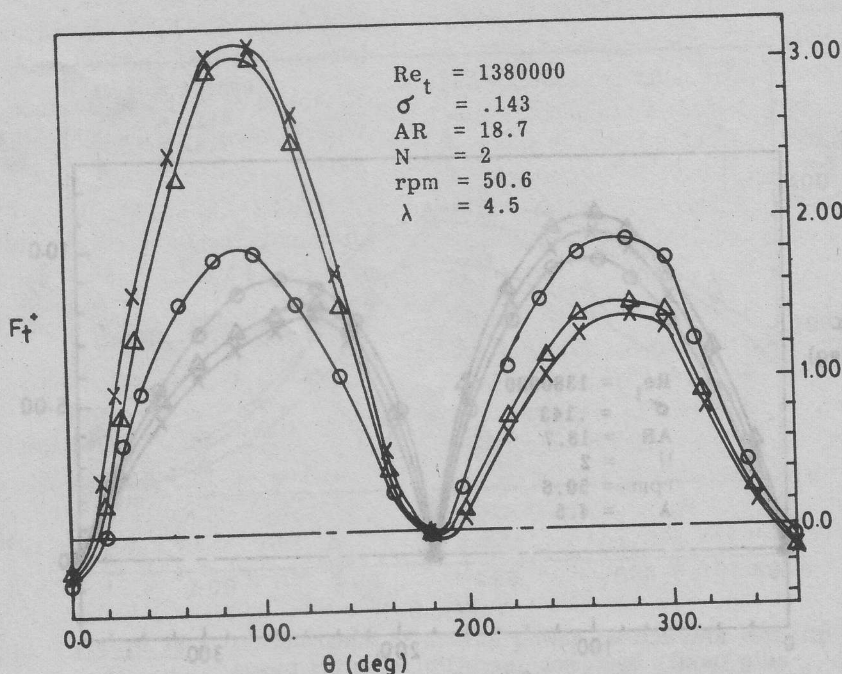

Figure 15 : Comparisons of local non-dimensional tangential forces.
Δ calc. (cascade theory ; NACA : 0015)
x calc. (cascade theory ; NACA : 1415)
o calc. (simple multiple streamtube theory; NACA:0015)

streamtube theory it is assumed that the induced velocities in the upstream and the downstream sides of the rotor are constant. But in the cascade theory for the upstream and the downstream sides these are calculated separately. In the cascade theory, the drop of axial velocity occurs twice one in the upstream side and another in the downstream side. The wake velocity in the upstream side acts as the inlet velocity in the downstream side. As a result the induced velocities in the upstream side are higher than those in the downstream side which is depicted in the figure 13. From this figure it is also observed that the induced velocity ratios calculated by cascade thoery for the blades of cambered cross-section varies in small amount in comparison with those calculated by cascade theory for the blades of symmetric cross-section. In the upstream side for the blade cross-section of cambered profile the lift value increases, making the higher blade element drag force in free stream velocity direction which is to be balanced by the higher drag produced due to the change of momentum and it occurs with the lower value of induced velocity.

It may be observed from the figure 14 that the local angles of attack by the cascade theory differ appreciably from those by simple multiple streamtube theory. But the local angle of attack values by the cascade theory for the blades of cambered cross-section differ in small amount from those by the cascade theory for the blades of symmetric cross-section. Figure 13 reveals that induced velocities in the upstream side fall for the cascade theory with blades of cambered cross-section than those for the cascade theory with blades of symmetric cross-section, which is the reason of relatively lower angles of attack in upstream side. Similarly angles of attack in the downstream sides may be explained.

Referring to the figures 15 and 16 for the comparative values of non-dimensional tangential and normal forces, one may observe that by cascade theory with blades of cambered cross-section and symmetric cross-section, the forces in the upstream side are higher than those in the downstream side while by the simple multiple streamtube theory, these forces are equal in both upstream and downstream sides. Figure 15 shows that higher forces are produced in the upstream side than those in the downstream side. This can be explained easily from the figure 14 showing angle of attack distribution. These angles are below the stalling angle, so for higher angle there is higher lift, hence higher tangential force and vice versa. Cascade theory with blades of cambered cross-section give relatively higher blade lift value which is the outcome of relatively higher local tangential force in the upstream side. Figure 16 showing local normal force distributions may be explained in the same manner as for the case of tangential force distribution in the figure 15.

4. CONCLUSIONS

Performance of a vertical axis straight bladed Darrieus turbine with blades of cambered cross-section improves but not in remarkable amount if compared to that of a Darrieus turbine with blades of symmetric cross-section.

Employing blades of cambered cross-section in place of symmetric cross-section, the local values of power increase in upstream side and decrease in downstream side in general.

Performance analysis has been made with the cascade theory mainly because the momentum theory fails to predict the performance at higher tip speed ratios, at higher solidities and higher blade pitchings.

REFERENCES

1. Hirsch, Ir. Ch. and Mandal, A. C., " A Cascade Theory for the Aerodynamic Performance of Darrieus Wind Turbines", Wind Engineering, England, Vol. 11, No. 3, 1987, pp. 164 - 175.
2. Clancy, L. J., " Aerodynamics", A Pitman International Text, 2nd Edition, 1978.
3. Abbott, H. and Von Doenhoff, A. E., " Theory of Wind Sections" Dover Publications, Inc. New York, 1959.
4. Hirsch Ir. Ch. and Mandal, A. C., " Flow Curvature Effect on Vertical Axis Darrieus Wind Turbine Having High Chord-Radius Ratios" , Proceedings of the 1st European Wind Energy Conference, Hamburg, Oct. 22-26, 1984, pp. G7- 407-410.
5. Jacobs, E. N. and Sherman, A., " Airfoil Characteristics as Affected by Variations of the Reynolds Number", NACA Report No. 586, 1937.
6. Wilmer, A. C., " Low Reynolds Number Tests on the NACA 0015 Section", Proceedings of the 1st European Wind Energy Workshop, April 1979, pp. 109-116.
7. Sharpe, D. J., " A Theoretical and Experimental Study of the Darrieus Vertical Axis Wind Turbine", School of Mechanical, Aeronautical & Production Engineering, Kingston Polytechnic, Research Report, October, 1977.